

Spherically symmetric configurations of General Relativity in presence of a scalar field: separation of test body circular orbits

O. S. Stashko and V. I. Zhdanov

Taras Shevchenko National University of Kyiv, Ukraine

(Dated: December 3, 2024)

We study test-body orbits in the gravitational field of a static spherically symmetric object in presence of a minimally coupled nonlinear scalar field. We generated a two-parametric family of scalar field potentials, which allow finding solutions of Einstein's equations in an analytic form. The results are presented by means of hypergeometric functions; they describe either a naked singularity (NS) or a black hole (BH). Our numerical investigation shows that in both cases the stable circular orbits can form separated (non-connected) regions around the configuration. We found existence conditions for such separated regions and present examples for some family parameters in case of NS and BH. The results may be of interest for testing models of the dynamical dark energy.

PACS numbers: 04.20.Jb 04.20.Dw 04.40.Dg, 04.50.Kd 04.70.Bw 97.10.Gz 97.60.Lf

Circular orbits around spherically symmetric configurations with scalar fields

I. INTRODUCTION AND BASIC RELATIONS

Scalar fields are often used in General Relativity, in particular to discuss the cosmological observations [1]. In theoretical models of a dynamical dark energy the "cosmological" scalar fields provide an inflationary stage of the early Universe (see, e.g., [1–3] for a review and references therein). One might think that effects of such fields on galactic scales are negligible at present epoch. Nevertheless, since the early works [4, 5], it is well known that any presence of a scalar field can cause a cardinal change of the space-time topology in the vicinity of a compact object.

The test body motion is probably a principal mean that can signal, by means of electromagnetic radiation, about the presence or absence of "non-canonical" effects related to scalar fields. The circular orbits around compact objects with scalar fields has been studied elsewhere [6, 7]. There is an interesting property of the space-time geodesic structure discovered in presence of the linear massless scalar field [7]: in this case there exist disconnected regions of stable circular orbits. Discontinuous structure of the orbits arises also owing to the presence of a quadrupole source [8]. One can suppose that such separated rings of orbits near relativistic compact objects is a widespread phenomenon in presence of the scalar fields (and maybe, in presence of the other fields). If such a separation really exists, this could affect considerably the form of the relativistic fluorescent iron lines generated in accretion disks, which are observed in active galactic nuclei (AGNs) [9–11]. This may be important for observations in order to test gravitational theories.

The present paper deals with test-body orbits in case of a family of spherically symmetric space-times of General Relativity, which describe static configurations in presence of a self-interacting scalar field. We derived exact special solutions of Einstein's equations using a known method (see, e.g., [12–16]) that allows one to generate asymptotically flat space-time metrics along with the corresponding scalar field potentials (Section II). We concentrate on solutions, which describe either a naked singularity (NS) or a black hole (BH) having a positive mass. Then we consider a test body motion in a static region (Section III) to find conditions for the existence of stable circular orbits. In particular, our numerical investigation shows that for some set of parameters of the problem there are disconnected

regions of stable circular orbits, which are separated by a region where a stable motion is impossible.

The action functional in presence of a self-interacting minimally coupled scalar field ϕ is

$$S = S_{GR} + \int d^4x \sqrt{|g|} \left[\frac{1}{2} g^{\mu\nu} \phi_{,\mu} \phi_{,\nu} - V(\phi) \right] , \quad (1)$$

where S_{GR} is the standard gravitational action of General Relativity ($c = 8\pi G = 1$), $V(\phi)$ is a self-interaction potential to be specified below. The metric of a spherically symmetric space-time can be written as

$$ds^2 = A(x) dt^2 - \frac{dx^2}{A(x)} - r^2(x) (d\theta^2 + \sin^2(\theta) d\phi^2) . \quad (2)$$

The Einstein's equations for this metric following from action (1) yield (see, e.g., [12],[14],[16]):

$$\frac{d}{dx} \left(\frac{dA}{dx} r^2 \right) = -2r^2 V(\varphi), \quad (3)$$

$$\frac{d^2 r}{dx^2} + \frac{1}{2} r \left(\frac{d\phi}{dx} \right)^2 = 0 \quad (4)$$

$$, \quad A \frac{d^2 r^2}{dx^2} - r^2 \frac{d^2 A}{dx^2} = 2 . \quad (5)$$

Variation of action (1) with respect to ϕ yields one more equation, which is not independent from equations (3—5); therefore, we do not write it. Equation (5) yields

$$A(x) = r^2(x) \int_x^\infty \frac{2x' - C}{r^4(x')} dx' , \quad (6)$$

where C is a constant. In view of (3),(4) we have

$$\phi(x) = \pm \int_x^\infty \sqrt{-\frac{2}{r} \frac{d^2 r}{dx^2}} , \quad (7)$$

and

$$V(x) = \frac{1}{r^2} - \frac{A}{r^2} \left(3 \left(\frac{dr}{dx} \right)^2 + r \frac{d^2 r}{dx^2} \right) - \frac{C - 2x}{r^3} \frac{dr}{dx} . \quad (8)$$

The system of equations (6—8) is equivalent to (3—5). On account of (6),(7) we can use the “inverse” method [12—17] to generate special solutions of this system: instead of looking for functions $A(x), r(x), \phi(x)$ for some given potential $V(\phi)$, we may fix any of these functions, for example $r(x)$, and look for $A(x), \phi(x)$ and $V(\phi)$. This problem is solved by quadratures according to (6),(7), (8); $V(\phi)$ is defined parametrically under condition $r^{-1} d^2 r / dx^2 < 0$.

II. FAMILY OF SOLUTIONS

Now we specify the problem to consider a family of solutions with

$$r(x) = x \left[1 - \left(\frac{x_0}{x} \right)^N \right], \quad N > 1. \quad (9)$$

Obviously, for $x > x_0$ we have $r > 0$, $d^2r/dx^2 < 0$, that is the conditions to apply the inverse method are fulfilled. We look for solutions that describe configurations with positive mass $m > 0$, i.e. having an asymptotic at large distances from the center $A(x) \approx 1 - 2m/x$. Using expansions of (6) in powers of x^{-1} (see (12) below), we have then $C = 6m$. Integration in (6) for $x > x_0$ yields $A(x)$ in terms of the hypergeometric function

$$A(x) = \left[1 - \left(\frac{x_0}{x} \right)^N \right]^2 \left\{ F \left[4, \frac{2}{N}, 1 + \frac{2}{N}, \left(\frac{x_0}{x} \right)^N \right] - \frac{C}{3x} F \left[4, \frac{3}{N}, 1 + \frac{3}{N}, \left(\frac{x_0}{x} \right)^N \right] \right\} \quad . \quad (10)$$

In view of (7) we have

$$\phi(x) = \pm \sqrt{\frac{8(N-1)}{N}} \arcsin \left[\left(\frac{x_0}{x} \right)^{N/2} \right]. \quad (11)$$

Formulas (8,10,11) define the potential $V(x)$ parametrically for $|\phi| < (\pi/2)\sqrt{8(N-1)/N}$ and correspondingly $x > x_0$. The potential $V(x)$ is explicitly derived using the functions $A(x), r(x)$ in (7,8), then we get $V(\phi)$ by a substitution of

$$x = x_0 \left\{ \sin \left(|\phi| \sqrt{\frac{N}{8(N-1)}} \right) \right\}^{-2/N}.$$

into $V(x)$.

Thus, we get a spherically-symmetric solutions of Einstein's equations with the scalar field in case of this potential; the solutions are given by (9,10,11).

Asymptotic relations at the spatial infinity are as follows

$$A(x) = 1 - \frac{C}{3x} + \frac{2(2-N)}{N+2} \left(\frac{x_0}{x} \right)^N + O(x^{-(N+1)}). \quad (12)$$

$$V(x) = \frac{N(N-1)(N-2)}{N+2} \frac{x_0^N}{x^{N+2}} + O(x^{-(N+3)}). \quad (13)$$

The scalar field self-interaction potential near the origin is similar for the NS and BH cases (see Fig. 1, left panel):

$$V(\phi) \approx \frac{(N-2)N^{2(1+1/N)}}{(N-1)^{2/N}(N+2)x_0^2} \left(\frac{|\phi|}{2\sqrt{2}} \right)^{2(1+2/N)}, \quad (14)$$

here we are dealing with massles scalar fields.

Using (6) and (9) we have in the neighborhood of x_0 :

the metric coefficient

$$A(x) = \frac{2x_0 - C}{3N^2(x - x_0)} + \frac{1}{N^2} \left[1 + \frac{2(N-1)(2x_0 - C)}{3x_0} \right] + O(x - x_0), \quad (15)$$

the potential

$$V(x) = -\frac{(N-1)(2x_0 - C)}{6N^2x_0(x - x_0)^2} - (N-1)\frac{7C - 5x_0 - 3CN + 6Nx_0}{3N^2x_0^2(x - x_0)} + O(1), \quad (16)$$

and the Ricci scalar

$$R = -T_{\mu\nu}g^{\mu\nu} = \frac{(N-1)(7C - 4x_0 - 3CN + 6Nx_0)}{N^2x_0^2(x - x_0)} + O(1). \quad (17)$$

If $2x_0 > C$, then for $x > x_0$ the integrand of (6) is positive and $A(x) > 0$. It is easy to show that the time needed for signals from the center $x = x_0$ to reach an external observer, is finite. Therefore we have NS at $x = x_0$. In this case the scalar field potential is not bounded from below. If $2x_0 < C$, then $A(x) \rightarrow -\infty$ for $x \rightarrow x_c + 0$, so $A(x)$ changes its sign at some point $x = x_{hor} > x_0$. According to [12] this is a simple horizon of BH.

The qualitative behavior of the solutions is consistent with the general results of [12], [16]. In both cases the potentials $V(\phi)$ are negative in some region (see examples in Fig. 1), so the solutions do not contradict to the no-scalar-hair theorems [12, 18]). In case of NS we have $V(\phi) \rightarrow -\infty$. In case of BH $V(\phi) \rightarrow \infty$ for $|\phi| \rightarrow \pi\sqrt{2(1 - 1/N)}$, here we have something like the "Mexican hat" potential (Fig. 1).

III. TEST BODY ORBITS

Further we use notations according to Fig. 2: the radial coordinates $x : x_3 < x < \infty$ correspond to the outer region of circular orbits, and $x : x_1 < x < x_2$ correspond to the inner region (if it exists), which is separated by a prohibited area $x_2 < x < x_3$ from the outer region.

In case of spherically symmetric space-time metrics (2) the integrals for the test body geodesic motion in the equatorial plane are as follows

$$A(x) \left(\frac{dt}{d\tau} \right) = p_t, \quad r^2(x) \left(\frac{d\varphi}{d\tau} \right) = L, \quad \theta = \pi/2,$$

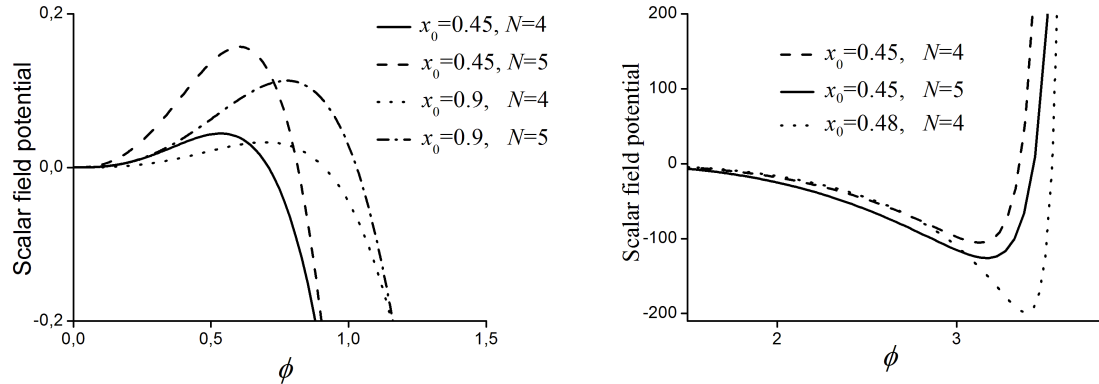


FIG. 1. Typical forms of the scalar field self-interaction potentials. Left panel: the cases of NS and BH for small ϕ , $N > 2$. Right panel: the cases of BH for larger ϕ showing the asymptotic behavior when $V(\phi) \rightarrow \infty$; the details near the origin are not visible on this scale.

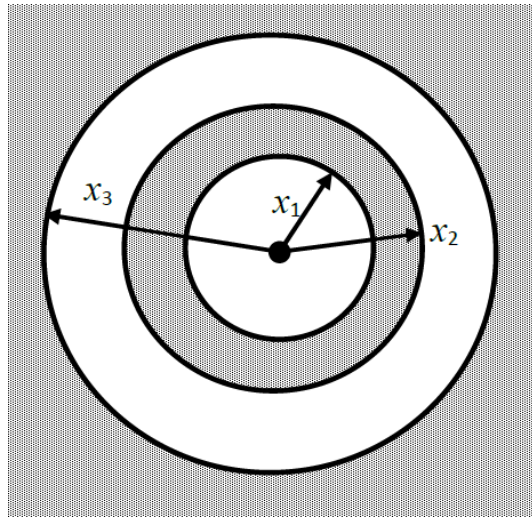


FIG. 2. Shaded area: regions of stable orbits. White area: no stable orbits.

τ — is the canonical parameter on the time-like geodesics. These equations together with the normalization integral yield the equation for the radial variable

$$\left(\frac{dx}{d\tau} \right)^2 = p_t^2 - V_{eff}(x), \quad V_{eff} = \alpha V_1 + V_2, \quad (18)$$

where

$$V_1(x) = \frac{A(x)}{r^2(x)} = 2 \int_x^\infty \frac{x' - 3m}{r^4(x')} dx', \quad V_2(x) = A(x), \quad \alpha = L^2. \quad (19)$$

Equation (18) formally describes a classical particle motion with energy $p_t^2/2$ in a field with effective potential $V_{eff}/2$. Minima of V_{eff} for some fixed $\alpha \geq 0$ correspond to stable circular

orbits (with some fixed angular momenta L), and the maxima – to unstable circular orbits that are limiting cycles for the test body trajectories. At the point of the minimum

$$\alpha V'_1 + V'_2 = 0. \quad (20)$$

In case of the Schwarzschild metric ($x_0 = 0, \phi \equiv 0, V \equiv 0$) there may be either one minimum $x_{min}(L)$ of V_{eff} and one maximum $x_{max}(L)$, or there is none. Here we shall look for situations when there may be two minima of V_{eff} .

Let us consider when additional minima can appear. The bifurcation parameter is α . At the bifurcation point (e.g., when the minimum/maximum appears or disappears) in addition to (20) we have

$$\alpha V''_1 + V''_2 = 0. \quad (21)$$

It follows from (20),(21) that the bifurcation values $\alpha = L^2$ (if they exist) must be determined from the formula $\alpha = -V'_2(X_r)/V'_1(X_r)$, where X_r is a root of the function

$$H(x) = V''_2(x) - V''_1(x)V'_2(x)/V'_1(x).$$

The explicit form of this function on account of (6) is

$$H(x) = 2 \left[\frac{r''(x)}{r(x)} + \frac{r'^2(x)}{r^2(x)} \right] A(x) - \frac{2}{r^2(x)} + \left[\frac{2r(x)r'(x)}{2x - C} A(x) - 1 \right] \cdot \left[\frac{4r'(x)}{r^3(x)} (2x - C) - \frac{2}{r^2(x)} \right]. \quad (22)$$

For $x \rightarrow x_0$ on account of (15) and (9) we have the asymptotic behavior:

$$H(x) \approx -\frac{2}{3} \frac{2x_0 - C}{N^2(x - x_0)^3}.$$

For $x \rightarrow \infty$ we have $H(x) \approx C/3x^3$.

IV. NUMERICAL RESULTS

For numerical estimates we choose further the units of length so as to have $C = 1$. Using zeros of $H(x)$ one can look for parameters $x_0 > 0, N > 1$ that lead to an appearance or disappearance of minima of V_{eff} for some α . After determination of roots X_r of $H(x)$ for fixed x_0, N we determine limiting values of angular momentum $L_{lim} = \sqrt{\alpha}$ according to (21) when additional minima of V_{eff} begin to appear. However, equation $H = 0$ (22) gives us a necessary (not sufficient) condition. In this view, we carried out a direct numerical check of the occurrence of these minima between different bifurcation points.

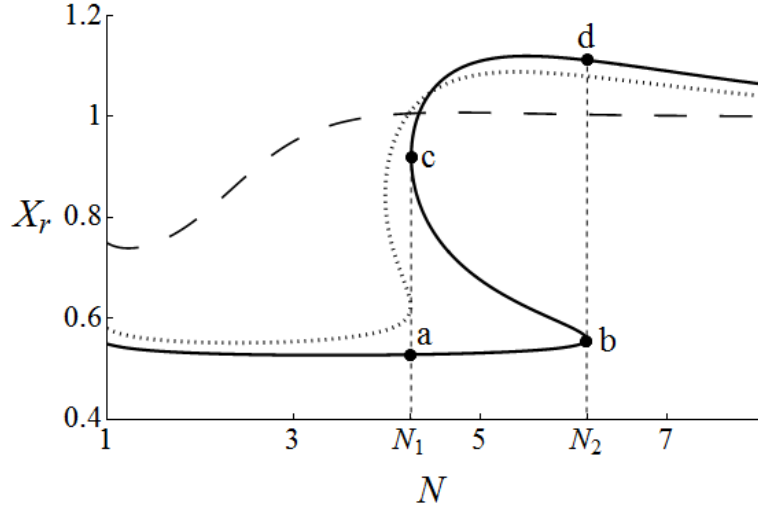


FIG. 3. Zeros $X_r(N)$ for three values of x_0 in the BH case. The dashed curve shows $X_r(N)$ for $x_0 = 0.25$, which defines the lower boundary of the stable circular orbit radii x_1 for different N . The case of $x_0 = 0.48$ (solid) represents a three-valued function between $N_1 \approx 4.3$ and $N_2 \approx 6.1$: the branch between points a and b represents $X_{r,1}(N)$, between b and c – $X_{r,2}(N)$ and between c and d – $X_{r,3}(N)$. The latter branch extends to infinity for $N > N_2$. The case of $x_0 = 0.42$ (dotted line) is intermediate; it shows how the curves transform as x_0 changes.

Further we present main results of the numerical investigation; they look different for BH ($x_0 < 0.5$) and NS ($x_0 \geq 0.5$). The dependences of boundary radii x_k , $k = 1, 2, 3$ upon N for some fixed values of x_0 are shown in Figs. 3, 4. Fig. 5 represents the dependence $x_k(x_0)$ for some fixed values of N .

(i) In case of BH $V_{eff}(x_{hor}) = 0$ at the horizon x_{hor} ; function $V_{eff}(x)$ is increasing in some neighborhood of x_{hor} . The type of monotony for $x > x_{hor}$ (and the occurrence of minima of $V_{eff}(x)$) depends on L, x_0, N . We studied this using roots X_r of $H(x)$.

We show in Fig. 3 how curves $X_r(N)$ are transformed as x_0 changes. For sufficiently small x_0 a typical situation is represented by the dashed curve $X_r(N)$ of this figure; here the dependence $X_r(N)$ single-valued. For every N there is the only root $X_r(N)$ that defines a lower boundary of stable orbit radii and a corresponding value of the limiting angular momentum L_{lim} . In this case there is the only connected region of stable circular orbits having different angular momenta. This region contains non-relativistic orbits with large x and correspondingly large L .

For larger x_0 the dependence $X_r(N)$ can be many-valued. Typical picture is represented

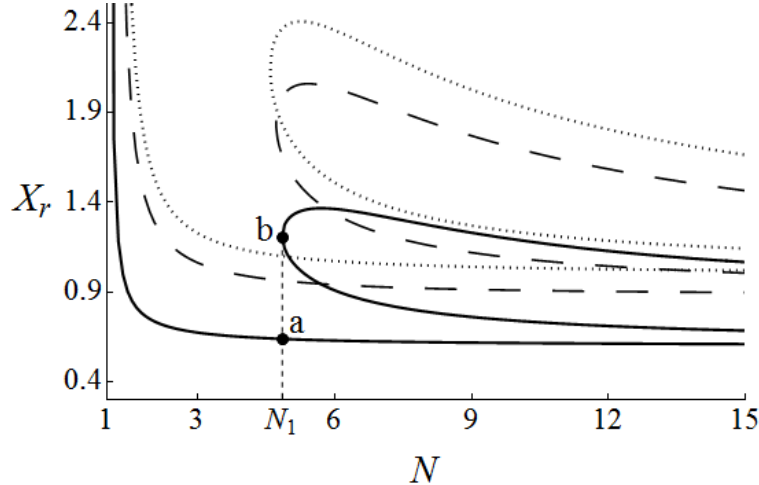


FIG. 4. The case of NS: dependencies $X_r(N)$ for $x_0 = 0.6$ (solid), $x_0 = 0.88$ (dashed): $x_0 = 1$ (dotted). The lower curves $x_1(N) \neq X_{r,1}(N)$ are derived from the condition of minimum of $A(x)$.

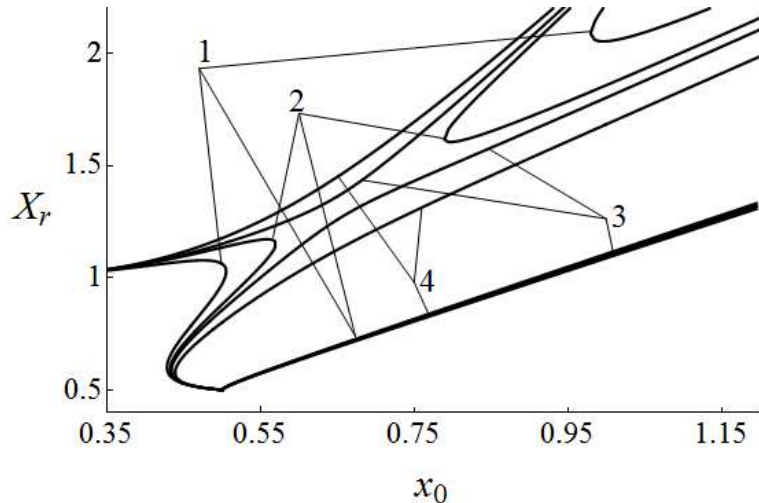


FIG. 5. $X_r(N)$ as a function of x_0 for different N in the neighborhood of a qualitative transition at $N = 4.87$: 1 – $N = 4.6$, 2 – $N = 4.8$, 3 – $N = 4.9$, 4 – $N = 5.2$. The lower curve for $x_0 > 0.5$ (the NS case) is actually made up of four different branches (1,2,3,4) of the boundary radii $x_1(N) \neq X_{r,1}$, which are almost merged together.

by the solid curve of Fig.3 for fixed $x_0 = 0.48$. For $N < N_1$ we have the only branch $X_{r,1}(N)$. For $N_1 < N < N_2$ there are three branches: $X_{r,1}(N) < X_{r,2}(N) < X_{r,3}(N)$ that are merged together at the points "b" and "c". For any fixed $N \in (N_1, N_2)$ these dependencies define two regions of the stable circular orbits: $\{x : x_1 = X_{r,1} < x < x_2 = X_{r,2}\}$, $\{x : x > x_3 = X_{r,3}\}$, and the intermediate region $x_1 < x < x_2$ is prohibited (cf. Fig. 2). For $N > N_2$ there is

again the only root $X_{r,3}(N)$.

To clarify the situation we show in Fig. 6 typical examples of effective potentials V_{eff} in case of BH ($x_0 = 4.5, N = 5$) and their derivatives dV_{eff}/dx . The figure illustrates how minima of V_{eff} emerge for different L and explicitly demonstrate that two minima of V_{eff} are indeed possible for some L . For all x_0, L , both bounded and unbounded motions are possible. In case of effective potentials of Fig. 6 we have three critical values of L ; there are stable circular orbits with radii $x \in [x_1, x_2]$ and $x \in [x_3, \infty)$, $x_2 < x_3$.

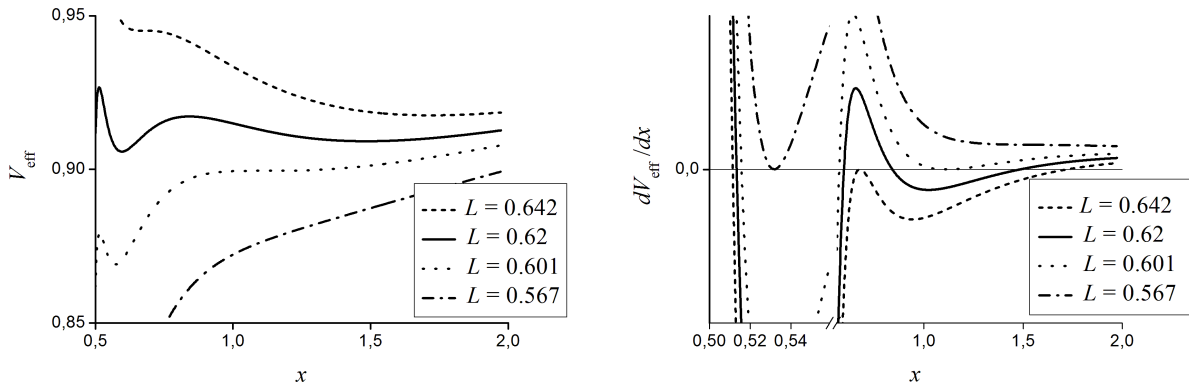


FIG. 6. The case of BH, $x_0 = 0.45, N = 5, C = 1$. In the left panel, effective potentials V_{eff} for critical values of the angular momentum: $L_1 = 0.567$ (dash-dot), $L_2 = 0.601$ (dotted), $L_3 = 0.642$ (dashed) when these graphs have inflection points. Right panel: the derivatives of these potentials; here the curves in interval $x \in (0.5, 0.55)$ (to the left of the break) are shown at a smaller scale. For $0 < L < L_1$ there is no minima of V_{eff} ; for $L_1 < L < L_2$ there is one minimum only. For $L > L_2$ an additional right minimum appears and both minima exist for $L \in [L_2, L_3]$, this is illustrated by the solid curves. For $L > L_3$ the left minimum disappears. Here L_1 corresponds to minimal radius of stable circular orbits $x_1 = 0.532$ (see Fig. 2 for the notations), L_2 – to $x_2 = 0.677$, L_3 – to $x_3 = 1.11$.

(ii) In case of NS ($x_0 \geq 0.5$) there also can be disconnected regions of the stable circular orbits. First of all we note that $V_{eff} \approx A(x) \approx -2m/x$ for $x \rightarrow \infty$ is monotonically increasing and taking into account asymptotic relation (15) we see that V_{eff} is decreasing near the center. Therefore, in case of NS there is always some minimum of V_{eff} for any L, x_0, N . In view of (18, 19) $A(x) = V_{eff}(L = 0)$. Analogously, $A(x)$ always has a minimum at some x_1 , which is a radial coordinate of a stationary particle that hangs at rest over the singularity. Our analysis shows that minima of $V_{eff}(L)$ for $L \neq 0$ are shifted to larger x

values. Therefore, x_1 is the lower boundary of stable circular orbit radii for all L . On the other hand, the left root $X_{r,1}(N)$ of $H(x)$ is unphysical (it leads to $L^2 < 0$).

Typical dependences $x_1(N)$ in the NS case are presented in Fig. 4. For N less than some N_1 this is the only branch of the limiting radii that extends to infinity. Starting from N_1 additional two branches appear, which can be calculated as roots of $H(x)$ ($X_{r,2}$ and $X_{r,3}$); these roots are physical and they indeed define boundaries of the stable orbits region for fixed x_0, N . As we see, the separated regions of orbits arise not for all parameters of the family.

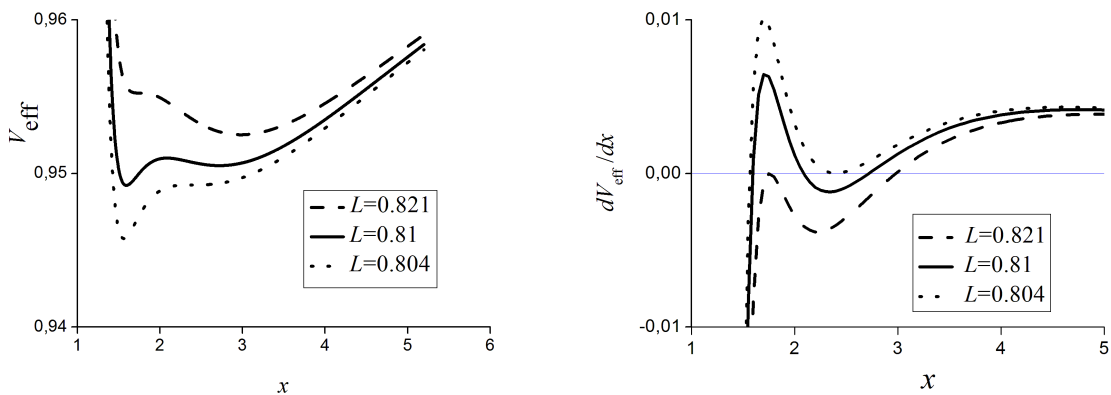


FIG. 7. The case of NS: $x_0 = 1, N = 5, C = 1$. Left panel: effective potentials V_{eff} for two critical values of L : 0.608 (dotted) $L = 0.627$ (dashed) and for the intermediate value (solid, $L = 0.62$). Right panel: the derivatives. The left minima of V_{eff} exist for angular momenta $L \in [0, 0.821]$. The right minima exist for $L \in [0.804, \infty]$. There is a common interval $L \in [0.804, 0.821]$ where two minima exist; the solid curve represents such an example. Correspondingly, for the boundary radii of the circular orbit regions we have $x_1 = 1.094, x_2 = 1.757, x_3 = 2.393$

As for dependences $x_k(x_0)$ plotted in Fig. 5, they also represent qualitatively different cases. For larger N there is an upper branch $x_3(x_0)$ that extends to all x_0 , and a continuous lower curve that consists of two parts, which are connected at the point $x_0 = 0.5$, where there is a discontinuity of the derivative. For $N < 4.87$ this curve is broken into two parts; the smaller N , the farther away is the right upper arm of the curve in the region of large x_0 . In the same way as in Fig. 4, the lower curve in Fig. 5 to the right of the break point also represents $x_1(x_0)$, not $X_{r,1}(x_0)$. The other curves in this figure are obtained as the roots X_r of $H(x)$.

In Fig. 7 we show a typical example of effective potentials with two minima in case of NS

$(x_0 = 1, N = 5)$, including the case with two minima for some L . The radii of the circular orbits that correspond to left and right minima belong to different intervals (x_1, x_2) and (x_3, ∞) (see Fig. 2 for the notations).

V. CONCLUSIONS

We derived a family of special solutions of the joint system of Einstein equations and massless scalar field equations with nonzero self-interaction potentials. We concentrated on the solutions that describe static spherically symmetric configurations having a positive total mass and corresponding asymptotically flat metric at spatial infinity. Some of these solutions deal with either NS in the center of the configuration, or with BH. The family includes the Schwarzschild metric as limiting case $x_0 = 0$.

The main outcome of this paper is that, for the solutions in question, separate (disconnected) ring-like structures of stable circular orbits can be formed. Analogous feature was first revealed in case of the massless scalar field without self-interaction [7]. We show that a similar result takes place for a massless nonlinear scalar field in case of the above family of solutions, including the BH case. We remind that the well-known no-hair theorem [18] does not work, if the scalar field potential is not positively definite; this is just the case of our solutions.

Evidently, our results dealing with a special family solutions do not describe the most general situation with the scalar field. Nevertheless, the results support the idea that the existence of separated ring-like regions in relativistic objects can be rather a common phenomenon in presence of the scalar field and/or some other fields of alternative gravitation theories. The presence of such ring-like structures in accretion disks around supermassive BHs can testify models of dark energy by means of the fluorescent iron lines (especially, Fe K α) in the X-ray spectra observed in AGNs [9–11]. The appearance of the ring-like structures in astrophysical objects could be detected on account of unusual deformations of the Fe K α lines. Of course, the scalar field effects, if they exist, will be obscured by less exotic ones, e.g., due to accretion disk warps in AGNs, inhomogeneous distributions of matter in the disks, reflection of X-rays from dust tori, and possible existence of BH companions (see, e.g., [19, 20]). Some additional information, that can reduce the number of unknowns in this problem, can be obtained in AGNs of gravitational lens systems [21].

On the other hand, there may be deformations in case of another kind of exotic objects [22]. This stimulates further observations and theoretical investigations of astrophysical compact objects in order to look for a smoking gun of the General Relativity modifications.

ACKNOWLEDGMENTS

This work has been fulfilled in the framework of the scientific research program "Astronomy and Space Physics" of Taras Shevchenko National University of Kyiv. Authors acknowledge the partial support of the State Foundation for Fundamental Research in Ukraine (project Ф64/45-2016).

[1] Plank collaboration. Planck 2013 results. XXII. Constraints on inflation. *Astron. Astrophys.* **571**, id.A22 (2014) [arXiv:1303.5082].

[2] A. Linde. Inflationary Cosmology after Planck 2013. ArXiv:1402.0526 (2014).

[3] B. Novosyadlyi, V. Pelykh, Yu. Shtanov, A. Zhuk. Dark energy and dark matter of the universe: in three volumes. Ed. V. Shulga. – Vol. 1: Dark matter: Observational evidence and theoretical models (Kiev, Akademperiodyka, 2013).

[4] I.Z. Fisher. Scalar mesostatic field with regard for gravitational effects. *Zh. Exp. Theor. Phys.* **18**, 636-640 (1948) [in Russian; English translation – arXiv:gr-qc/9911008].

[5] A.I. Janis, E.T. Newman, J. Winicour. Reality of the Schwarzschild singularity. *Phys. Rev. Lett.*, **20**, 878-880 (1968).

[6] D. Solovyev, A. Tsirulev. General properties and exact models of static self-gravitating scalar field configurations. *Classical Quantum Gravity* **29**, id.055013 (2012).

[7] A.N. Chowdhury, M. Patil, D. Malafarina, P.S. Joshi. Circular geodesics and accretion disks in the Janis-Newman-Winicour and gamma metric spacetimes. *Phys. Rev. D* **85**, id. 104031 (2012) [arXiv:1112.2522].

[8] K. Boshkayev, E. Gasperín, A.C. Gutiérrez-Piñeres, H. Quevedo, S. Toktarbay. Motion of test particles in the field of a naked singularity. *Phys. Rev. D* , **93**, id.024024 (2016) [arXiv:1509.03827].

- [9] P.W. Guilbert, M.J. Rees. “Cold” material in non-thermal sources. *Mon. Notic. Roy. Astron. Soc.* **233**, 475-484 (1988).
- [10] A.P. Lightman, T.R. White. Effects of cold matter in active galactic nuclei - A broad hump in the X-ray spectra. *Astrophys. J.* **335**, 57-66 (1988).
- [11] A.C. Fabian, M.J. Rees, L. Stella, N.E. White. X-ray fluorescence from the inner disc in Cygnus X-1 // *Mon. Notic. Roy. Astron. Soc.* **238**, 729-736 (1989).
- [12] K.A. Bronnikov. Spherically symmetric false vacuum: no-go theorems and global structure. *Phys. Rev. D* **64**, id.064013 (2001) [arXiv:gr-qc/0104092].
- [13] K.A. Bronnikov , G.N. Shikin. Spherically Symmetric Scalar Vacuum: No-Go Theorems, Black Holes and Solitons. *Gravitation Cosmol.* **8**, 107–116 (2002) [arXiv:gr-qc/0109027].
- [14] K.A. Bronnikov. J.C. Fabris. Regular phantom black holes. *Phys. Rev. Lett.* **96**, id.251101 (2006) [arXiv:gr-qc/0511109].
- [15] V.V. Nikonov, Ju.V. Tchemarina, A.N. Tsirulev. A two-parameter family of exact asymptotically flat solutions to the Einstein-scalar field equations. *Classical Quantum Gravity* **25**, id. 138001 (2008).
- [16] M. Azreg-Aïnou, Selection criteria for two-parameter solutions to scalar-tensor gravity. *General Relativity Gravit.* **42**, 1427-1456 (2010) [arXiv:0912.1722].
- [17] M. Cadoni, E. Franziny, Asymptotically flat black holes sourced by a massless scalar field. *Phys. Rev. D* **91**, id. 104011 (2015) [arXiv:1503.04734].
- [18] J.D. Bekenstein, Black Holes: Classical Properties, Thermodynamics and Heuristic Quantization. ArXiv:gr-qc/9808028 (1998).
- [19] A.A. Vasylenko, E.V. Fedorova, B.I. Hnatyk, V.I. Zhdanov. Evidence for a binary black hole in active nucleus of NGC 1194 galaxy? *Kinemat. Phys. Celest. Bodies.* **31**, 13–18 (2015).
- [20] E. Fedorova, A. Vasylenko, B.I. Hnatyk, V.I. Zhdanov. The peculiar megamaser AGN NGC 1194: Comparison with the warped disk candidates NGC 1068 and NGC 4258. *Astronom. Nachr.* **337**, 96-100 (2016).
- [21] A. Neronov, Ie. Vovk. Test of relativistic gravity using microlensing of relativistically broadened lines in gravitationally lensed quasars. *Phys. Rev. D* **93**, id.023006 (2016).
- [22] C. Bambi, D. Malafarina. K α iron line profile from accretion disks around regular and singular exotic compact objects. *Phys. Rev. D* **88**, id. 064022 (2013).